Annals of Nuclear Energy 94 (2016) 399–408

Contents lists available at ScienceDirect

Annals of Nuclear Energy

journal homepage: www.elsevier.com/locate/anucene

Nuclear data uncertainty propagation analysis for depletion calculation in PWR and FR pin-cells

Tiejun Zu, Chao Yang, Liangzhi Cao *, Hongchun Wu

School of Nuclear Science and Technology, Xi'an Jiaotong University, Xi'an, Shaanxi 710049, China

ARTICLE INFO

Article history:
Received 3 January 2016
Received in revised form 5 April 2016
Accepted 9 April 2016
Available online 16 April 2016

Keywords:
Nuclear data
Sensitivity analysis
Uncertainty propagation
Depletion calculation

ABSTRACT

In order to assess the nuclear data uncertainty propagation in the depletion calculation, a computational code named SUNDEW has been developed based on the home-developed lattice code NECP-CACTI. In the SUNDEW, Generalized Perturbation Theory (GPT) is applied to calculate sensitivity coefficients of response function with respect to the nuclear cross sections. Method of Characteristics (MOC) is employed to solve the transport equation, adjoint and generalized adjoint transport equations. Chebyshev Rational Approximation Method (CRAM) is implemented to solve the depletion equation and adjoint depletion equation. The sensitivity coefficients of K_{eff} and nuclide density with respect to the nuclear cross sections are verified by comparing with the results of direct perturbation calculation. The uncertainties on K_{eff} and the nuclide density at different depletions, which are induced by the nuclear cross sections uncertainties, are analyzed based on ENDF/B-VII.1 covariance data for LWR and fast reactor pin-cells. The numerical results show that there are significant differences between LWR and fast reactor pin-cells. The differences are mainly caused by the differences of the sensitivity coefficients between the LWR and fast reactor pin-cells. In addition, to identify the cross section improvement priority for nuclides, reactions and energy ranges, the dominant contributors to K_{eff} and nuclide density uncertainties are analyzed at different depletions.

1. Introduction

The accurate prediction of nuclear parameters in depletion calculation is of great significance for the management of spent nuclear fuel, core design, and even economy and safety of nuclear reactor. However, the reliability of neutron transport and depletion calculations is subject to some degree of uncertainties due to a lot of approximations made in the computational model and inaccuracy of input parameters. Traditionally, conservative safety margins are used in safety analysis of reactor because the uncertainties are not quantified. Reasonable safety margins, which are conducive to improve the economy of reactor, can be given if the uncertainties are quantified.

The nuclear cross sections are used as basic input data for the neutron transport and depletion calculations, whose uncertainties are likely one of the most significant sources of uncertainties of response functions (Pusa, 2012a,b). Therefore, the interest towards sensitivity and uncertainty analysis with respect to the nuclear cross sections has increased markedly in recent years. With the larger availability of covariance files, as in the ENDF/B-VII.1 library (Chadwick et al., 2011), the JENDL4.0 (Shibata et al., 2011) and TENDL-2009 libraries (Koning and Rochman, 2009), the uncertainty quantification of the response function using covariance data prepared in these nuclear data libraries has been carried out by two different approaches: stochastic sampling method and first order generalized perturbation method. The stochastic sampling method can get a probability distribution of output with different input data samples. The probability distribution characterizes the uncertainty related to output. This method is easy to be implemented by running existing transport and depletion codes with different input data samples, but at the expense of high computational costs. It has been carried out in XSUSA/SCALE (Zwermann et al., 2012), TMC/SERPENT (Rochman et al., 2012) and NUDUNA (Diez et al., 2015). In the first order perturbation method, the uncertainty of the response function is quantified with the sensitivity coefficient regarding to input parameters by error propagation formulation. The formulation to calculate the sensitivity coefficient was proposed by Takeda based on a differential approach in 1985 (Takeda and Umano, 1985). This approach employs first order approximation but can provide the sensitivity coefficient, which only requires one time forward depletion calculation and one time adjoint depletion calculation. It is very efficient when the number of considered response functions is not too large.

* Corresponding author.
E-mail address: caolz@mail.xjtu.edu.cn (L. Cao).

http://dx.doi.org/10.1016/j.anucene.2016.04.006
0306-4549/

So it is applicable for the sensitivity and uncertainty analysis in the pin-cell micro-depletion calculation. Up to now, however, most uncertainty studies based on the first order perturbation method have different levels of approximations, such as neglecting the nuclide density uncertainties induced by the nuclear cross sections uncertainties in the depletion calculation (Oak Ridge National Laboratory, 2009) or neglecting the flux uncertainties (Aliberti et al., 2002), or based on diffusion theory (Yokoyama, 2014).

In order to make a comprehensive assessment, the sensitivity and uncertainty analysis is carried out based on the first order perturbation method in this paper. Both the nuclide density uncertainties and flux uncertainties induced by the uncertainties of the nuclear cross sections in the depletion calculation are considered. The transport code is used to obtain the flux, which can make the result more reliable. A new code named SUNDEW is developed. The SUNDEW code is verified by comparing with the result of direct perturbation (DP) calculation.

In 2006, the NEA/OECD Uncertainty Analysis in Modeling (UAM) workshop established a depletion benchmark for propagating cross section uncertainties in LWR design and safety calculations, and the objective was to address the uncertainty induced by the basic nuclear data in the depletion calculation (Ivanov et al., 2012). In 2008, the NEA/OECD Working Party on Evaluation Cooperation (WPEC) Subgroup 26 published a report, which pointed out that a comprehensive sensitivity and uncertainty analysis should be performed to evaluate the impact of nuclear cross sections uncertainties on the significant integral parameters of innovative systems, even beyond the Gen-IV range of systems (Salvatores and Jacqmin, 2008). Nowadays, the neutronics experience with UO_2 fuel and thermal reactors such as Light Water Reactors (LWR) is extremely extensive, but nuclear data uncertainties are still one of the most significant sources of uncertainties of neutronics calculations. For fast reactor, most nuclear data are available in modern data files, but their accuracy and validation are still a major concern. It is widely accepted that the uncertainties of nuclear data for fast reactor design should still be significantly reduced (Palmiotti et al., 2009). In this paper, the SUNDEW code is used to perform the nuclear data uncertainty propagation analysis for a LWR burn-up pin-cell benchmark proposed by the NEA/OECD (Ivanov et al., 2012) and a fast reactor (FR) burn-up pin-cell to assess the effect of nuclear data uncertainties on a different system with a fast spectrum. The uncertainties of K_{eff} and the nuclide densities at different depletions are analyzed based on the ENDF/B-VII.1 covariance data. In addition, to identify the cross section improvement priority for nuclide, reaction and energy range, the dominant contributors of K_{eff} and nuclide density uncertainties are analyzed.

The organization of this paper is as follows: Section 2 describes the theoretical models of this work. The calculation results of sensitivity coefficient and uncertainty analysis associated with the LWR and FR pin-cells are given in Section 3. Finally, conclusions are provided in Section 4.

2. Uncertainty propagation methodology

The depletion analysis consists of two components: transport calculation and depletion calculation. The transport calculation is used to calculate fluxes and prepare weighted cross sections with updated nuclide densities. Microscopic reaction rates estimated at the beginning of a depletion step are used to solve depletion equation to update the nuclide density at the end of the depletion step. So the transport calculation and depletion calculation have a strong relationship. Any data perturbations which affect one will also affect the other. The first order perturbation method taking account of the nuclide density uncertainties and flux uncertainties induced by the nuclear cross sections in the depletion calculation is introduced in this section.

2.1. Depletion sensitivity coefficient theory

The sensitivity coefficient of R with respect to the nuclear cross section is expressed by

$$S^k_{x,g,z} = \frac{dR}{R} \Big/ \frac{d\sigma^k_{x,g,z}}{\sigma^k_{x,g,z}} \tag{1}$$

where k, x, g, and z are the indices of nuclide, reaction type, neutron energy group and region, respectively.

In the depletion analysis, the calculated nuclear response functions R, such as K_{eff} or nuclide density ($\mathbf{N}$), are a function of the nuclear cross sections (σ), nuclide density, neutron flux ($\mathbf{\Phi}$), and adjoint neutron flux ($\mathbf{\Phi}^*$). Namely, the R can be written as

$$R = f(\sigma, \mathbf{N}, \mathbf{\Phi}, \mathbf{\Phi}^*) \tag{2}$$

Expanding the left-hand side of Eq. (1) with a function Taylor series and neglecting the higher-order terms:

$$S^k_{x,g,z} = \frac{\sigma^k_{x,g,z}}{R}\left(\frac{\partial R}{\partial \sigma^k_{x,g,z}} + \frac{\partial R}{\partial \mathbf{N}}\frac{d\mathbf{N}}{d\sigma^k_{x,g,z}} + \frac{\partial R}{\partial \mathbf{\Phi}}\frac{d\mathbf{\Phi}}{d\sigma^k_{x,g,z}} + \frac{\partial R}{\partial \mathbf{\Phi}^*}\frac{d\mathbf{\Phi}^*}{d\sigma^k_{x,g,z}}\right) \tag{3}$$

In reactor design studies, it is frequently desired to determine the response functions that are time-dependent. So the R is represented as integration over all depletion period from t_0 (the beginning of depletion period) to t_f (the end of depletion period). Assuming that $\mathbf{\Phi}$ and $\mathbf{\Phi}^*$ are constant in each depletion step, Eq. (3) can be written as

$$\begin{aligned} S^k_{x,g,z} = \frac{\sigma^k_{x,g,z}}{R}\Bigg(&\int_{t_0}^{t_f}\frac{\partial R}{\partial \sigma^k_{x,g,z}}dt + \int_{t_0}^{t_f}\frac{\partial R}{\partial \mathbf{N}}\frac{d\mathbf{N}}{d\sigma^k_{x,g,z}}dt \\ &+ \sum_{i=0}^{I-1}\frac{d\mathbf{\Phi}_i}{d\sigma^k_{x,g,z}}\int_{t_i}^{t_{i+1}}\frac{\partial R}{\partial \mathbf{\Phi}_i}dt + \sum_{i=0}^{I-1}\frac{d\mathbf{\Phi}^*_i}{d\sigma^k_{x,g,z}}\int_{t_i}^{t_{i+1}}\frac{\partial R}{\partial \mathbf{\Phi}^*_i}dt + \frac{\partial R}{\partial \mathbf{N}_I}\frac{d\mathbf{N}_I}{d\sigma^k_{x,g,z}} \\ &+ \frac{\partial R}{\partial \mathbf{\Phi}_I}\frac{d\mathbf{\Phi}_I}{d\sigma^k_{x,g,z}} + \frac{\partial R}{\partial \mathbf{\Phi}^*_I}\frac{d\mathbf{\Phi}^*_I}{d\sigma^k_{x,g,z}}\Bigg) \end{aligned} \tag{4}$$

where i is the index of the depletion step; I is the total number of steps; t_i and t_{i+1} are the beginning and end of the ith depletion step, respectively.

Depletion analysis is to solve three coupled equations which are given by Eqs. (5)–(7)

$$\frac{d\mathbf{N}_i(t)}{dt} = \mathbf{M}_i\mathbf{N}_i(t) \tag{5}$$

$$\mathbf{B}_i\mathbf{\Phi}_i = 0 \tag{6}$$

$$P_i = \int_V \sum_k \kappa^k \boldsymbol{\sigma}^k_f N^k_i \mathbf{\Phi}_i dV \tag{7}$$

$$\mathbf{B}^*_i\mathbf{\Phi}^*_i = 0 \tag{8}$$

where Eq. (5) is the depletion equation; Eq. (6) is the neutron transport equation; Eq. (7) is the equation of power calculation; $\mathbf{M}_i$ is the transmutation matrix containing the rate coefficients for neutron absorption and radioactive decay; $\mathbf{B}_i$ is the multi-group transport operator; P_i is the total power over core volume; κ^k is the energy released per fission for nuclide k; $\boldsymbol{\sigma}^k_f$ is the microscopic fission cross section for nuclide k; Eq. (8) is the adjoint transport equation; $\mathbf{B}^*_i$ is the adjoint operator of $\mathbf{B}_i$.

In this paper, a formulation for calculating depletion sensitivity coefficients is derived according to the variation method described

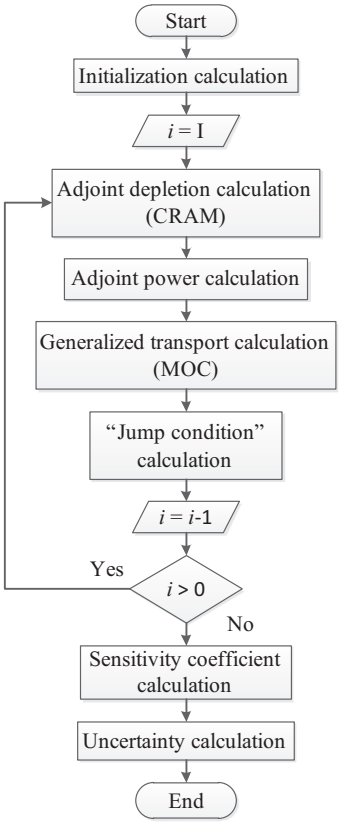

Fig. 1. Calculation flow diagram for SUNDEW.

by TAKEDA (Takeda and Umano, 1985). The final formulation for calculating depletion sensitivity coefficients can be expressed by

$$S^k_{x,g,z}=\frac{\sigma^k_{x,g,z}}{R}\left(\int_{t_0}^{t_f}\frac{\partial R}{\partial\sigma^k_{x,g,z}}dt+\sum_{i=0}^{I-1}\int_{t_i}^{t_{i+1}}\mathbf{N}^*\frac{\partial\mathbf{M}}{\partial\sigma^k_{x,g,z}}\mathbf{N}dt+\sum_{i=0}^{I}\boldsymbol{\Gamma}^*_i\frac{\partial\mathbf{B}_i}{\partial\sigma^k_{x,g,z}}\boldsymbol{\Phi}_i+\sum_{i=0}^{I}\boldsymbol{\Gamma}_i\frac{\partial\mathbf{B}^*_i}{\partial\sigma^k_{x,g,z}}\boldsymbol{\Phi}^*_i-\sum_{i=0}^{I}P^*_i\frac{\partial P_i}{\partial\sigma^k_{x,g,z}}\right)\tag{9}$$

In Eq. (9), the **N**, **M**, **B**, **B***, **Φ**, **Φ*** and P are calculated at each depletion point in the forward depletion analysis, while the **N***, **Γ**, **Γ*** and P^* can be solved through Eqs. (10)–(18) at different depletions.

$$P^*_I=\int_E\int_V\Phi_I\frac{\partial R}{\partial\Phi_I}dEdV/P_I\tag{10}$$

$$\mathbf{B}_I\boldsymbol{\Gamma}_I=-\frac{\partial R}{\partial\boldsymbol{\Phi}^*_I}\tag{11}$$

$$\mathbf{B}^*_I\boldsymbol{\Gamma}^*_I=\sum_k P^*_I\kappa^k\sigma^k_f N^k_I-\frac{\partial R}{\partial\Phi_I}\tag{12}$$

Table 1
Nuclide density for FR pin-cell.

Zone	Nuclides	Nuclide density
Fuel	^{235}U	2.674e−03
	^{236}U	1.218e−04
	^{238}U	1.527e−02
	^{239}Pu	3.184e−04
	^{240}Pu	1.002e−05
	^{241}Pu	2.633e−07
	^{242}Pu	2.633e−07
	^{90}Zr	2.242e−02
Cladding	^{52}Cr	1.347e−02
	^{56}Fe	5.377e−02
	^{58}Ni	7.619e−03
	^{95}Mo	1.648e−03
Coolant	^{23}Na	2.214e−02

$$N^{*k}_I=\boldsymbol{\Gamma}_I\frac{\partial\mathbf{B}^*_I}{\partial N^k_I}\boldsymbol{\Phi}^*_I+\boldsymbol{\Gamma}^*_I\frac{\partial\mathbf{B}_I}{\partial N^k_I}\boldsymbol{\Phi}_I-\kappa^k\sigma^k_f P^*_I\Phi_I+\frac{\partial R}{\partial N^k_I}\tag{13}$$

$$-\frac{d\mathbf{N}^*(t)}{dt}=\mathbf{M}^T_i\mathbf{N}^*(t)+\frac{\partial R}{\partial\mathbf{N}(t)}\tag{14}$$

$$\mathbf{B}_i\boldsymbol{\Gamma}_i=\int_{t_i}^{t_{i+1}}\frac{\partial R}{\partial\boldsymbol{\Phi}^*_i}dt\tag{15}$$

$$\mathbf{B}^*_i\boldsymbol{\Gamma}^*_i=-\int_{t_i}^{t_{i+1}}\left(\mathbf{N}^*\frac{\partial\mathbf{M}}{\partial\Phi_i}\mathbf{N}+\frac{\partial R}{\partial\Phi_i}\right)dt+P^*_i\sum_k\kappa^k\sigma^k_f N^k_i\tag{16}$$

$$P^*_i=\int_E\int_V\int_{t_i}^{t_{i+1}}\left(\mathbf{N}^*\mathbf{M}\mathbf{N}+\Phi_i\frac{\partial R}{\partial\Phi_i}\right)dtdVdE\Big/P_i\tag{17}$$

$$N^{*k-}_i=N^{*k+}_i+\left(\boldsymbol{\Gamma}_i\frac{\partial\mathbf{B}^*_i}{\partial N_i}\boldsymbol{\Phi}^*_i+\boldsymbol{\Gamma}^*_i\frac{\partial\mathbf{B}_i}{\partial N_i}\boldsymbol{\Phi}_i-\kappa^k\sigma^k_f P^*_i\boldsymbol{\Phi}_i\right)\tag{18}$$

where $N^{*k-}_i=N^{*k}_i(t^-_i)$; $N^{*k+}_i=N^{*k}_i(t^+_i)$; $\mathbf{M}^T_i$ is the transpose of $\mathbf{M}_i$; Eq. (14) is the adjoint depletion equation; Eq. (15) is the generalized transport equation; Eq. (16) is the generalized adjoint transport equation. The solution of Eq. (15) is zero when the response function is K_{eff} or the nuclide density. The detailed process to solve Eqs. (14) and (16) is introduced in Section 2.3.

2.2. Uncertainty

In the first order perturbation method for sensitivity and uncertainty analysis, uncertainty can be obtained through the sandwich rule after sensitivity coefficients are computed. The uncertainty on R can be evaluated as follows:

$$\frac{\Delta R^2}{R^2}=\mathbf{S}_{R(\boldsymbol{\sigma})}\,\mathbf{C}(\boldsymbol{\sigma})\mathbf{S}^T_{R(\boldsymbol{\sigma})}\tag{19}$$

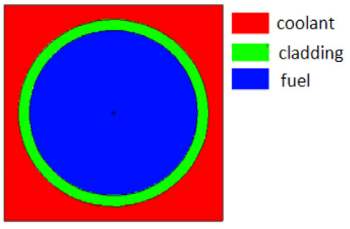

Parameter	Value
Cell pitch/mm	7.95
Fuel diameter/mm	6.1
Fuel material	U-Pu-Zr
Cladding thickness/mm	0.4
Coolant material	Na

Fig. 2. Specification of the fast reactor pin-cell.

where $S_{R(\sigma)}$ is the vector of sensitivity coefficients of R with respect to the cross section vector $\boldsymbol{\sigma}$; $\mathbf{S}^T_{R(\sigma)}$ is the transpose of $\mathbf{S}_{R(\sigma)}$; $\mathbf{C}(\boldsymbol{\sigma})$ is the covariance matrix of $\boldsymbol{\sigma}$, which is generated by NJOY based on the ENDF/B-VII.1 (Chadwick et al., 2011) library in this paper.

2.3. Implementation

A home-developed lattice code named NECP-CACTI (Li et al., 2015), is applied to perform the forward depletion analysis. The resonance calculation module is carried out based on the subgroup method; the Method of Characteristic (MOC) is employed to solve the transport equation Eq. (6); the Chebyshev Rational Approximation Method (CRAM) is implemented to solve the depletion equation Eq. (5). The MOC is also employed to solve the adjoint transport equation Eq. (8) and generalized adjoint transport equation Eq. (16). Before the adjoint transport calculation, the following modifications need to be implemented (Pusa, 2012a,b):

(1) Transpose the scattering matrix.
(2) Invert the group indices.
(3) Interchange the vectors $\bar{\nu}\boldsymbol{\sigma}_f$ and $\boldsymbol{\chi}$.

After these modifications, the MOC method is used to solve Eq. (8). When solving the generalized adjoint transport equation Eq. (16), the following modifications need to be additionally performed:

(1) Add the external source S_g

$$S_g = -\int_{t_i}^{t_{i+1}} \left(\mathbf{N}^* \frac{\partial \mathbf{M}}{\partial \Phi_{i,g}} \mathbf{N} + \frac{\partial R}{\partial \Phi_{i,g}} \right) dt + P_i^* \sum_k \kappa^k \sigma_{f,g}^k N_i^k \tag{20}$$

(2) Modify the adjoint fission source F_g^*

$$F_g^* = \frac{\overline{\nu}\Sigma_{f,g}}{4\pi k} \sum_{g'=1}^{G} \chi_{g'} \left(\Gamma_{g'}^* - \frac{\langle \mathbf{F}^* \boldsymbol{\Gamma}^*, \boldsymbol{\Phi} \rangle}{\langle \mathbf{F}^* \boldsymbol{\Phi}^*, \boldsymbol{\Phi} \rangle} \Phi_{g'}^* \right) \tag{21}$$

where $\boldsymbol{\Phi}$ denotes the solution of Eq. (6) and $\boldsymbol{\Phi}^*$ is the solution of Eq. (8); $\mathbf{F}^*$ is the multi-group adjoint fission operator. After these modifications, Eq. (16) can be solved by the MOC method.

By comparing Eq. (14) with Eq. (5), it can be seen that the two equations would be of same form if the depletion equation have an external source. For the case where R is a delta function at t_f, Eq. (14) is equivalent to (Williams, 1978)

$$\begin{cases} -\frac{d\mathbf{N}^*(t)}{dt} = \mathbf{M}_i^T \mathbf{N}^*(t) & t_0 \leqslant t < t_f \\ \mathbf{N}(t_f) = \frac{\partial R}{\partial \mathbf{N}_{t_f}} & t = t_f \end{cases} \tag{22}$$

In this case, the CRAM may be used to solve Eq. (14) with that modification transposing the transmutation matrix.

The adjoint depletion calculation is carried out by a code named SUNDEW. The computational flow of SUNDEW is shown in Fig. 1. It can be seen that the computational flow is very similar to that for the forward depletion calculation, excepting that the SUNDEW

Table 2
Sensitivity coefficients of K_{eff} in LWR pin-cell.

0 GWd/tU			20 GWd/tU			40 GWd/tU		
Reactions	Sundew	DP	Reactions	Sundew	DP	Reactions	Sundew	DP
^{235}U (υ)	0.936	0.936	^{235}U (υ)	0.584	0.584	^{239}Pu (υ)	0.437	0.437
^{238}U (n, γ)	−0.275	−0.274	^{239}Pu (υ)	0.305	0.305	^{235}U (υ)	0.373	0.373
^{235}U (n, f)	−0.264	−0.264	^{238}U (n, γ)	−0.241	−0.240	^{239}Pu (n, f)	0.199	0.203
^{1}H (scat)	0.206	0.205	^{1}H (scat)	0.234	0.224	^{1}H (scat)	0.184	0.161
^{235}U (n, γ)	−0.155	−0.155	^{239}Pu (n, f)	0.135	0.135	^{239}Pu (n, γ)	−0.168	−0.174

Table 3
Sensitivity coefficients of K_{eff} in FR pin-cell.

0 GWd/tU			20 GWd/tU			40 GWd/tU		
Reactions	Sundew	DP	Reactions	Sundew	DP	Reactions	Sundew	DP
^{235}U (υ)	0.774	0.774	^{235}U (υ)	0.697	0.698	^{235}U (υ)	0.622	0.622
^{235}U (n, f)	0.447	0.447	^{235}U (n, f)	0.374	0.374	^{235}U (n, f)	0.303	0.304
^{238}U (n, γ)	−0.246	−0.246	^{238}U (n, γ)	−0.197	−0.197	^{239}Pu (υ)	0.260	0.261
^{239}Pu (υ)	0.113	0.113	^{239}Pu (υ)	0.187	0.187	^{238}U (n, γ)	−0.148	−0.148
^{238}U (υ)	0.109	0.109	^{239}Pu (n, f)	0.111	0.111	^{239}Pu (n, f)	0.145	0.145

Table 4
Sensitivity coefficients of nuclide density of ^{244}Cm in LWR pin-cell.

Depletion	10 GWd/tU		20 GWd/tU		30 GWd/tU		40 GWd/tU	
Reactions	Sundew	DP	Sundew	DP	Sundew	DP	Sundew	DP
^{235}U (n, f)	−3.337	−3.114	−2.782	−2.543	−2.293	−2.083	−1.877	−1.695
^{235}U (n, γ)	0.296	0.262	0.289	0.255	0.287	0.254	0.286	0.254
^{238}U (n, γ)	0.805	0.827	0.511	0.522	0.251	0.257	0.015	0.016
^{239}Pu (n, f)	−0.352	−0.327	−0.595	−0.568	−0.743	−0.711	−0.833	−0.796
^{239}Pu (n, γ)	1.017	1.001	1.021	0.992	1.002	0.969	0.979	0.941
^{240}Pu (n, γ)	0.827	0.800	0.674	0.643	0.557	0.528	0.465	0.439
^{241}Pu (n, f)	−0.078	−0.077	−0.170	−0.167	−0.266	−0.262	−0.357	−0.352
^{241}Pu (n, γ)	0.978	0.971	0.958	0.949	0.940	0.929	0.922	0.911
^{242}Pu (n, γ)	0.962	0.967	0.929	0.929	0.889	0.886	0.843	0.839
^{243}Am (n, γ)	0.947	0.951	0.895	0.896	0.837	0.837	0.776	0.775
^{244}Cm (n, γ)	−0.015	−0.015	−0.033	−0.033	−0.054	−0.055	−0.078	−0.079

Table 5
Sensitivity coefficients of nuclide density of ^{244}Cm in FR pin-cell.

Depletion	10 GWd/tU		20 GWd/tU		30 GWd/tU		40 GWd/tU	
Reactions	Sundew	DP	Sundew	DP	Sundew	DP	Sundew	DP
^{235}U (n, f)	−1.843	−1.841	−1.745	−1.744	−1.651	−1.650	−1.561	−1.561
^{235}U (n, γ)	−0.089	−0.087	−0.075	−0.072	−0.061	−0.057	−0.047	−0.042
^{238}U (n, f)	−0.195	−0.195	−0.195	−0.196	−0.196	−0.197	−0.196	−0.198
^{238}U (n, γ)	−0.370	−0.367	−0.418	−0.412	−0.466	−0.458	−0.515	−0.504
^{239}Pu (n, f)	−0.263	−0.264	−0.294	−0.295	−0.324	−0.325	−0.353	−0.355
^{239}Pu (n, γ)	−0.010	−0.010	−0.010	−0.010	−0.009	−0.009	−0.008	−0.007
^{242}Pu (n, γ)	0.997	0.996	0.993	0.992	0.989	0.988	0.984	0.983
^{243}Am (n, γ)	0.986	0.987	0.972	0.973	0.958	0.960	0.944	0.946

Table 6
Uncertainty of K_{eff} at different depletions.

Depletion (GWd/tU)	0	10	20	30	40	50	60
Uncertainty for LWR cell (%)	0.508	0.495	0.484	0.462	0.437	0.423	0.434
Uncertainty for FR cell (%)	2.305	2.340	2.375	2.406	2.434	2.456	2.473

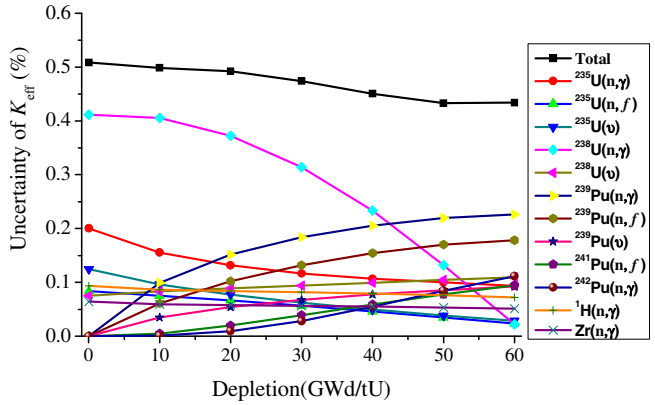

Fig. 3. Contributors of some important reactions uncertainties to K_{eff} uncertainty in LWR pin-cell.

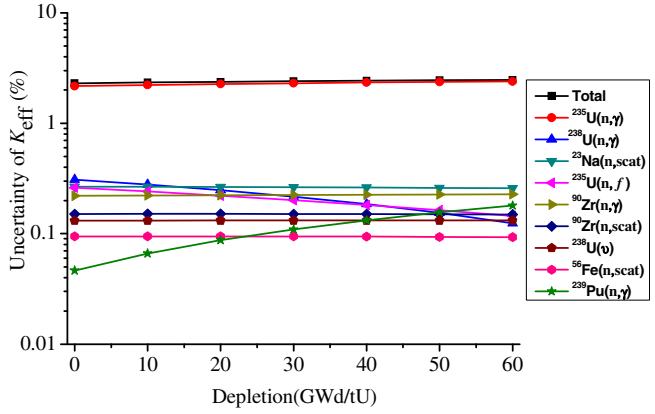

Fig. 4. Contributors of some important reactions uncertainties to K_{eff} uncertainty in FR pin-cell.

calculation proceed backward in time. The main following flow chart is given as follow:

(1) At the end of depletion period, the P_I^*, $\mathbf{\Gamma}_I$ and $\mathbf{\Gamma}_I^*$ are determined from Eqs. (10)–(12), then initial value of $\mathbf{N}_I^*$ is calculated from Eq. (13).
(2) The value of $\mathbf{N}^*(t)$ is solved from Eq. (14) based on the CRAM method (Pusa and Leppanen, 2010) for the present depletion interval. The partial fraction decomposition coefficients for the CRAM approximation of order 14 were taken in this paper (Pusa, 2012a,b).
(3) Adjoint power (P_i^*) is calculated by using of Eq. (17) based on the assumption that the change of $\mathbf{N}(t)$ and $\mathbf{N}^*(t)$ is linear during the present depletion interval.
(4) Then the MOC method is used to determine $\mathbf{\Gamma}_i$ and $\mathbf{\Gamma}_i^*$ based on Eqs. (15) and (16) at $t = t_i$.
(5) The adjoint nuclide density distribution has a discontinuity between the present and next depletion interval. The initial value of $\mathbf{N}^*(t)$ is calculated in accordance with Eq. (18) for the next depletion step, the second term on the right hand side of Eq. (18) represents a "jump condition" on $\mathbf{N}^*(t)$ at $t = t_i$.
(6) Go to the (2).

If the quantities $\mathbf{N}^*, \mathbf{\Gamma}^*, \mathbf{\Gamma}$ and P^* are calculated at all depletions, the depletion sensitivity coefficients can be determined easily in accordance with Eq. (9). Finally, the uncertainty can be quantified using the sandwich rule. In addition, the lattice code NECP-CACTI is based on a cross section model, where the individual reactions have been combined to a total reaction. For instance, the total scattering reaction consists of elastic and inelastic reactions. However, the covariance data are reported for the individual reactions in the ENDF/B-VII.1 library. To assess the uncertainties of total scattering and capture reaction, the relative covariance data for the total reaction must be computed. Generally, the total scattering or capture cross section is defined as the sum of the individual scattering or capture cross sections. The expression can be written in matrix form as

$$\boldsymbol{\sigma}_{x,t} = \sum_{mt} \boldsymbol{\sigma}_{x,mt} = \mathbf{S}\boldsymbol{\sigma} \tag{23}$$

where $\boldsymbol{\sigma}_{x,t}$ is the total cross section for x-type reaction, such as the scattering or capture reaction. $\boldsymbol{\sigma}_{x,mt}$ are the individual cross sections for the x-type reaction. Since the relationship between $\boldsymbol{\sigma}_{x,t}$ and $\boldsymbol{\sigma}$ is linear, the absolute covariance matrix of $\boldsymbol{\sigma}_{x,t}$ can be obtained with the sandwich rule

$$\mathbf{C}(\boldsymbol{\sigma}_{x,t}) = \mathbf{S}\mathbf{C}(\boldsymbol{\sigma})\mathbf{S}^T \tag{24}$$

The corresponding total cross section relative covariance matrix can be easily calculated by dividing the absolute covariance matrix elements $\mathbf{C}_{ij}$ by $\boldsymbol{\sigma}_i\boldsymbol{\sigma}_j$. The EPRI-CPM 69-group structure (MacFarlane and Muir, 1994) is used for the LWR pin-cell in this paper, so corresponding 69-group structure cross section library and covariance library are created using NJOY based on the ENDF/B-VII.1. For the FR pin-cell, the cross section library is generated using OpenMC based on the ENDF/B-VII.1 (Du et al., 2014). The VITAMIN-J175-group structure (MacFarlane and Muir, 1994) is employed, and the corresponding 175-group structure covariance library is created using NJOY based on the ENDF/B-VII.1.

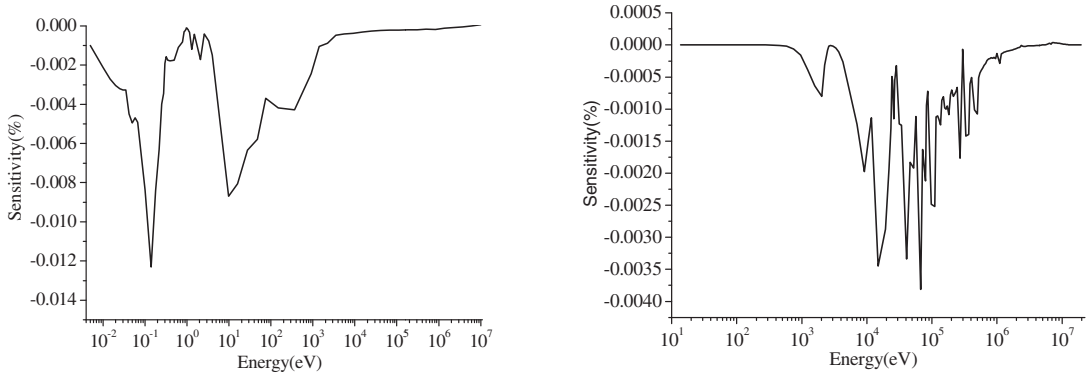

Fig. 5. Sensitivity coefficient of K_{eff} with respect to the ^{235}U (n, γ) in different pin-cell.

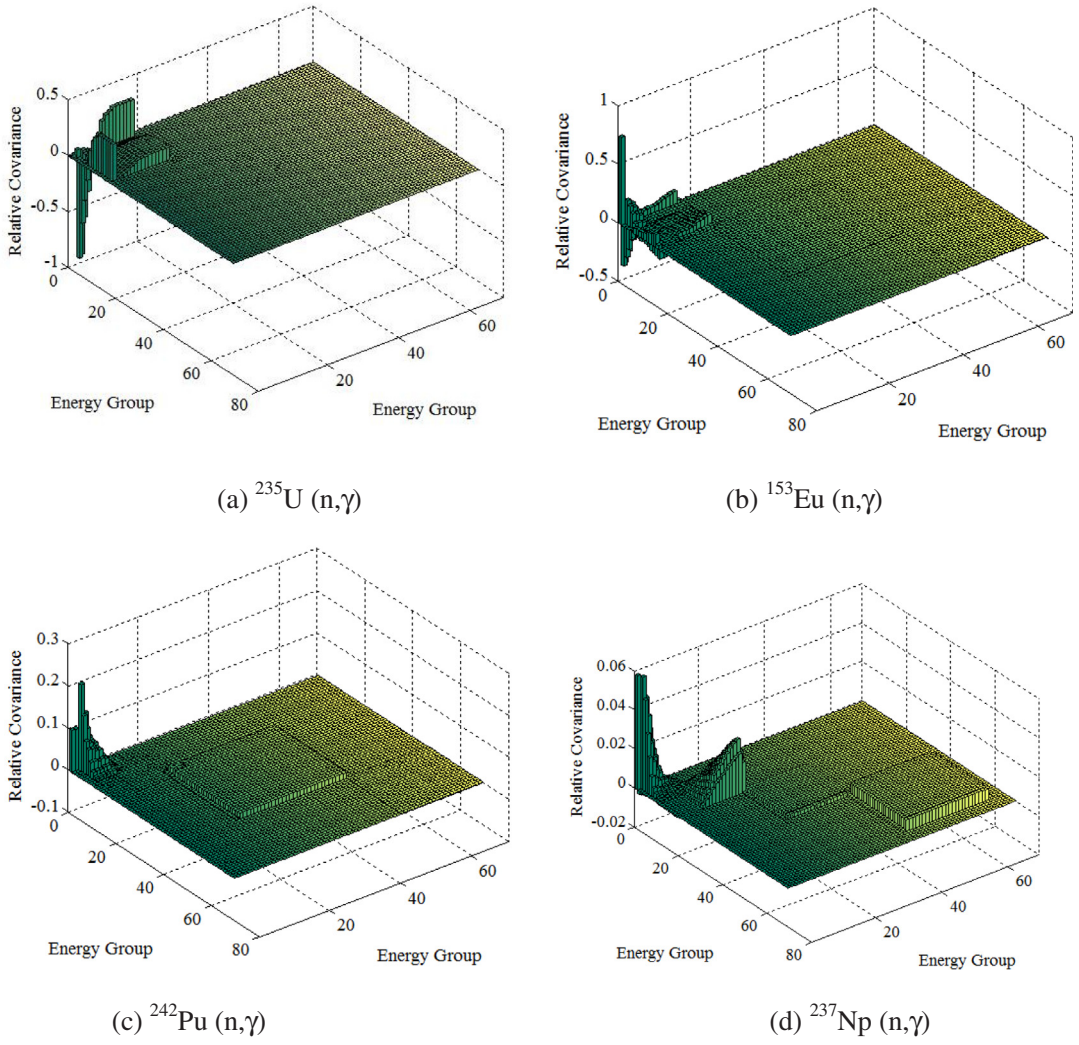

Fig. 6. 69-Group covariance data for different nuclear cross sections.

3. Numerical verification and analysis

3.1. Numerical verification

To verify the SUNDEW code, the sensitivity coefficients calculated with the SUNDEW are compared with reference sensitivity coefficients calculated with the DP, which are obtained by numerical differentiation in which a relative perturbation of 1% is given to a specific nuclear cross section (Rearden, 2004). A LWR pin-cell and FR pin-cell is used for the verification. The LWR burn-up pin-cell benchmark proposed by the NEA/OECD is used to perform the sensitivity and uncertainty study on a typical LWR in this paper (Ivanov et al., 2012). The Hot Full Power conditions are selected in this paper, where the average power density is 33.58 W/gU. For the FR pin-cell, the main specifications are summarized in Fig. 2. The nuclide density for each zone is given in

Table 7
Uncertainties of nuclide density at different depletions.

Depletion	10 GWd/tU		30 GWd/tU		50 GWd/tU	
Isotopes	LWR cell	FR cell	LWR cell	FR cell	LWR cell	FR cell
^{95}Mo	0.06	0.30	0.19	0.34	0.34	0.40
^{99}Tc	0.04	0.28	0.08	0.32	0.15	0.41
^{109}Ag	1.20	0.42	1.37	0.66	1.78	0.94
^{134}Cs	3.11	6.18	3.13	8.97	3.25	9.75
^{135}Cs	0.31	0.28	0.56	0.31	0.87	0.36
^{143}Nd	0.29	0.31	0.94	0.34	1.69	0.40
^{145}Nd	0.28	0.30	0.95	0.34	1.74	0.42
^{149}Sm	4.90	0.43	5.02	1.14	5.32	1.93
^{151}Sm	4.71	0.70	5.73	2.06	6.07	3.49
^{131}Xe	0.95	0.28	3.00	0.30	5.16	0.34
^{155}Eu	24.46	0.25	27.13	0.58	28.06	1.06
^{154}Gd	4.97	19.98	4.43	19.45	3.75	18.89
^{155}Gd	23.96	0.21	25.84	0.47	25.28	0.83
^{156}Gd	0.87	0.39	1.96	0.90	3.33	1.33
^{157}Gd	4.19	0.30	4.47	0.42	4.87	0.58
^{158}Gd	0.73	0.33	0.74	0.47	0.58	0.61
^{234}U	0.13	0.26	0.43	0.83	0.80	1.43
^{235}U	0.08	0.39	0.48	1.27	1.41	2.31
^{236}U	1.39	6.46	1.36	12.94	1.31	16.11
^{238}U	0.01	0.01	0.03	0.03	0.05	0.05
^{237}Np	1.47	2.42	2.49	5.27	3.05	7.88
^{238}Pu	4.39	6.39	4.05	7.26	4.04	8.55
^{239}Pu	1.66	0.52	2.09	0.88	2.65	0.95
^{240}Pu	1.92	2.07	2.14	4.31	2.44	5.24
^{241}Pu	1.95	1.78	1.82	4.03	2.21	5.32
^{242}Pu	2.86	0.26	3.01	1.18	4.01	2.83
^{241}Am	2.14	1.01	2.72	2.71	4.08	4.05
^{243}Am	11.45	4.04	10.34	3.90	9.05	3.94
^{244}Cm	12.09	7.88	11.12	7.47	9.95	7.19

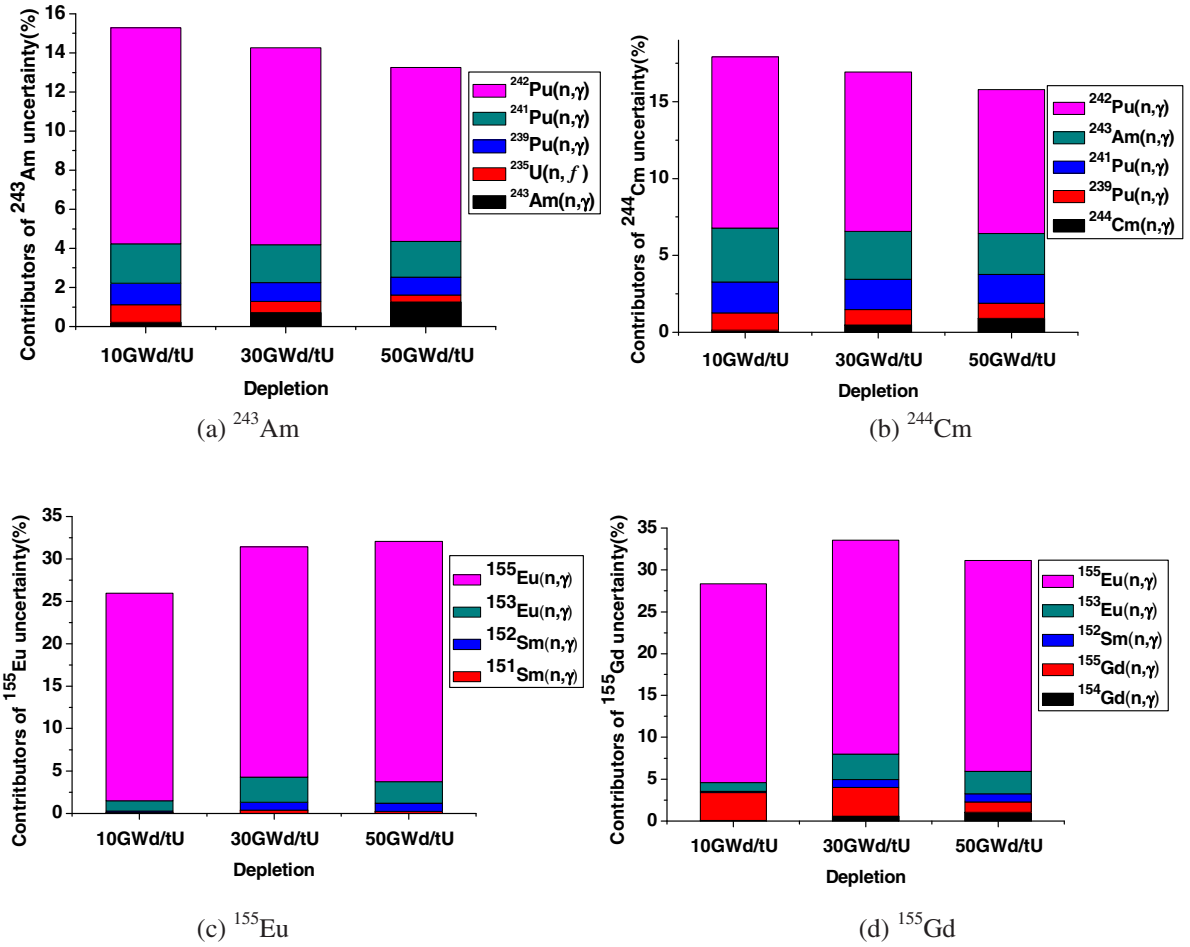

Fig. 7. Contributors of uncertainties on nuclide densities at different depletions in LWR pin-cell.

Table 1. The average power density is 64.36 W/gU during the whole depletion period.

The sensitivity coefficients of K_{eff} and nuclide density of ^{244}Cm with respect to some important nuclear cross sections are analyzed for the LWR and FR pin-cells.

Tables 2 and 3 show the top five sensitivity coefficients of K_{eff} with respect to the nuclear reactions at 0, 20 and 40 GWd/tU, respectively. From the results, it can be seen that the calculation results of SUNDEW agree well with those of DP method. For the LWR pin-cell, K_{eff} is more sensitive to the cross sections of ^{235}U and ^{238}U at beginning of lifetime. With the depletion of uranium and accumulation of plutonium, the K_{eff} becomes more sensitive to the cross sections of ^{239}Pu. Moreover, the sensitivity coefficient of K_{eff} with respect to the scatter cross section of ^{1}H is considerable. Similarly, K_{eff} is also more sensitive to the cross sections of ^{235}U and ^{238}U at the beginning of lifetime for the FR pin-cell. With the depletion of uranium and accumulation of plutonium, the sensitivity coefficient of K_{eff} to the cross sections of ^{235}U and ^{238}U decreases gradually, and increases slowly to the cross sections of plutonium.

Tables 4 and 5 show verification results of sensitivity coefficients of nuclide density of ^{244}Cm with respect to the different cross sections at different depletions. It can be seen that the calculation results of the SUNDEW agree well with those of the DP for the LWR and FR pin-cell.

3.2. Uncertainty analysis of K_{eff}

Table 6 shows the K_{eff} uncertainty assessment that is obtained based on the ENDF/B-VII.1 covariance data. The covariance data for prompt neutron multiplicities (υ_p) of ^{235}U is applied to assess the total neutron multiplicities (υ_t) to the uncertainty of K_{eff}, because the difference between the covariance data of υ_p and υ_t is too large to be explained by the delayed neutron multiplicities (Diez et al., 2015). The total uncertainty of K_{eff} at the beginning of the lifetime amounts to 508pcm and approximately 430 pcm at 60 GWd/tU for the LWR pin-cell. For the FR pin-cell, the total uncertainty on K_{eff} is approximately 2300 pcm at the beginning of the lifetime, which increases gradually with the depth of depletion.

Fig. 3 presents the contributions of some important nuclide reactions uncertainties to the K_{eff} uncertainty at different depletions for the LWR pin-cell. From the results, it can be seen that the K_{eff} uncertainty mainly comes from the nuclear cross section of ^{235}U and ^{238}U at beginning of lifetime, especially the capture cross section of ^{238}U. With the depletion of uranium and accumulation of plutonium, the uncertainties induced by the plutonium nuclear cross section become the dominant contributor to the K_{eff} uncertainty. Fig. 4 presents the contributions of some important nuclide reactions uncertainties to the K_{eff} uncertainty at different depletions for the FR pin-cell. It can be found that the K_{eff} uncertainty is mainly caused by the uncertainties of ^{235}U (n, γ), ^{23}Na (n, scat) and ^{90}Zr (n, γ) during the whole of lifetime. Similarly, with the depletion of uranium and accumulation of plutonium, the uncertainties induced by the plutonium nuclear data become larger slowly. There is crucial difference between the LWR and FR pin-cells for the K_{eff} uncertainty induced by the ^{235}U (n, γ). This is principally because the sensitivity coefficient of K_{eff} with respect to the ^{235}U (n, γ) is very different for the LWR and FR pin-cell. As shown in Fig. 5, the K_{eff} is more sensitive to the ^{235}U (n, γ) at the lower energy range for the LWR pin-cell. However, it is more

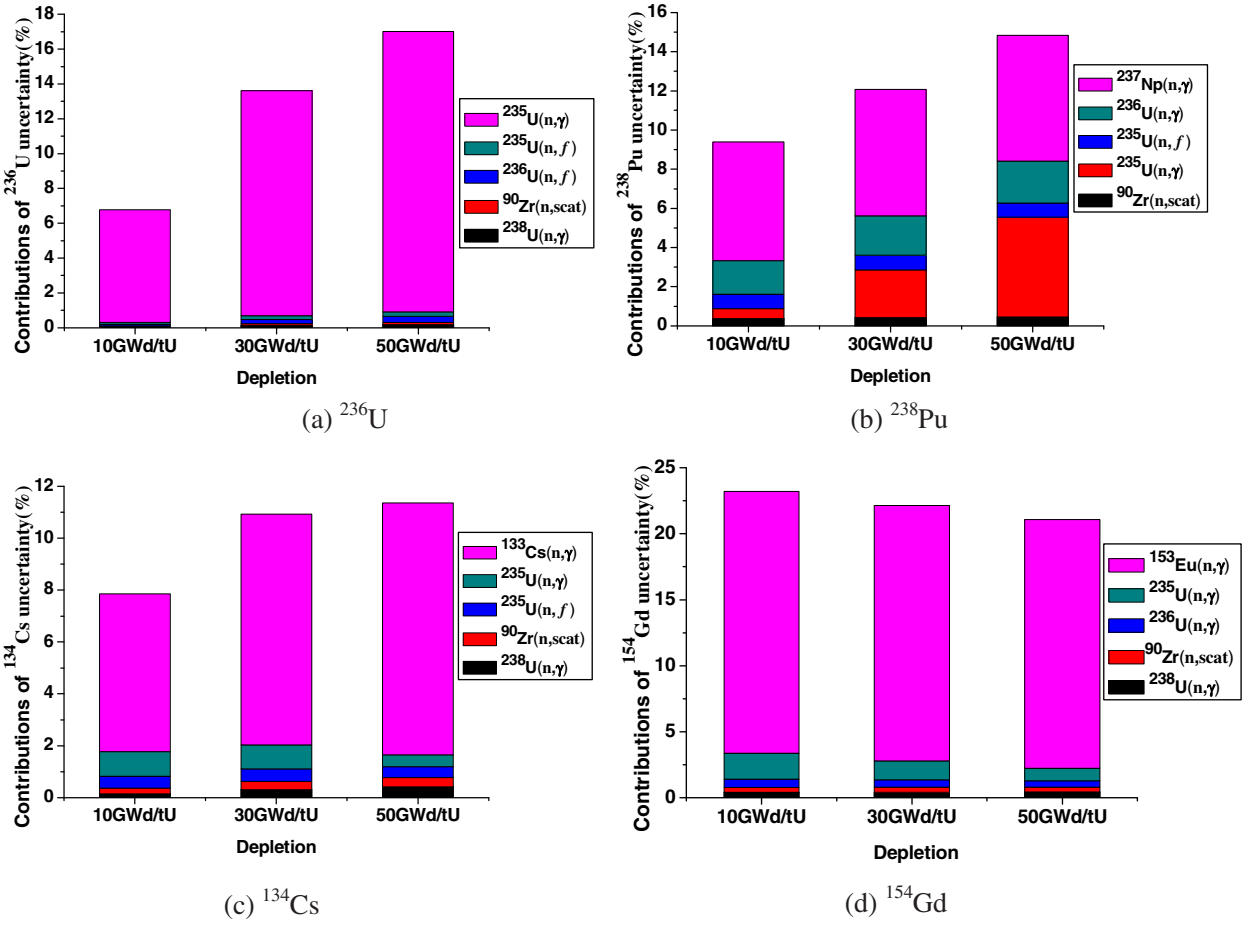

Fig. 8. Contributors of uncertainties on nuclide densities at different depletions in FR pin-cell.

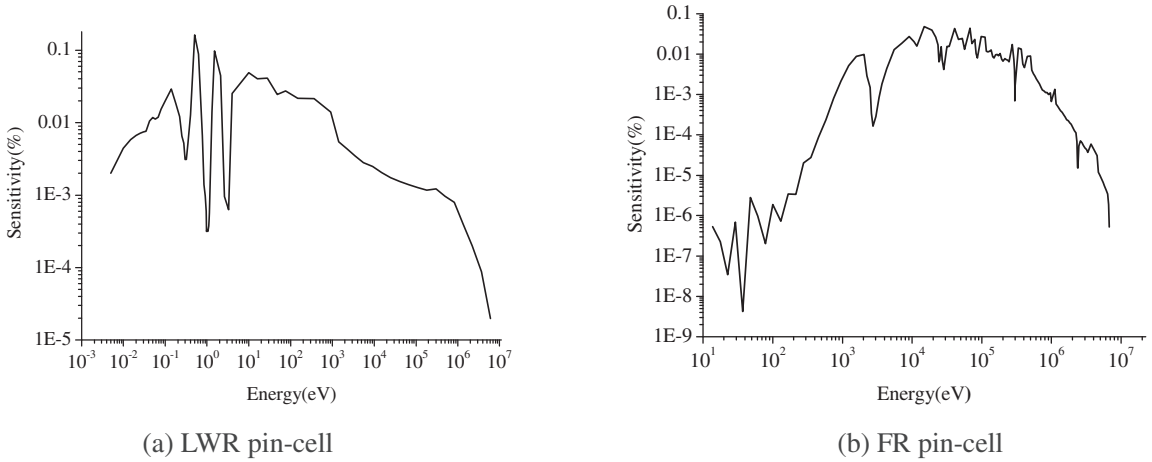

Fig. 9. Sensitivity coefficient of nuclide density of ^{238}Pu with respect to ^{237}Np (n, γ).

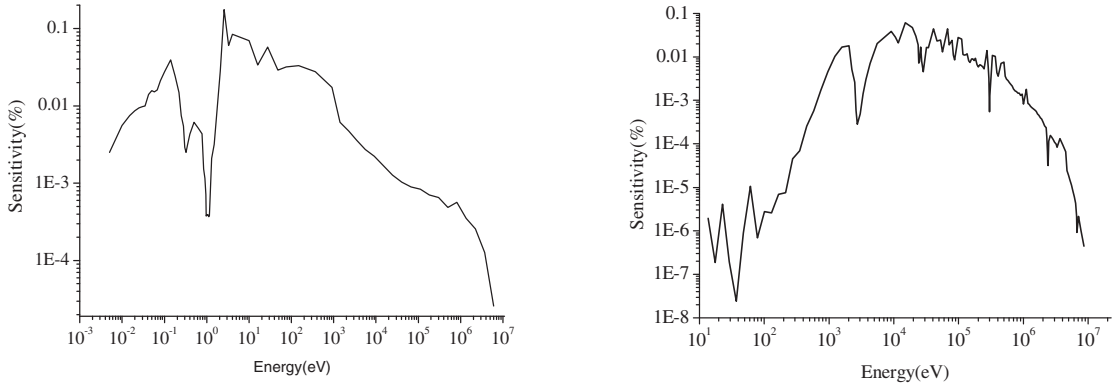

Fig. 10. Sensitivity coefficient of nuclide density of ^{154}Gd with respect to ^{153}Eu (n, γ).

sensitive at the higher energy range for FR pin-cell. Fig. 6(a) presents the covariance data of ^{235}U (n, γ), which is obviously larger at the higher energy range than at the lower energy range, so the K_{eff} uncertainty induced by the ^{235}U (n, γ) is larger in the FR pin-cell than that in the LWR pin-cell.

3.3. Uncertainty analysis of nuclide density

The uncertainties of nuclide density at different depletions are presented in Table 7. For the LWR pin-cell, the uncertainties of uranic and transuranic isotopes are less than 5% during the whole depletion period. Two exceptions are ^{243}Am and ^{244}Cm for their uncertainties amount to 11.45% and 12.09%, respectively. The uncertainties of fission products stay below 7%, except that ^{155}Eu and ^{155}Gd, and their uncertainties amount to 28.06% and 25.84%, respectively. For the FR pin-cell, the uncertainties of the most of heavy isotopes are larger than those in the LWR pin-cell. The uncertainty of ^{236}U is up to 16.11%. The uncertainties of fission products are less than 4%, except that ^{134}Cs and ^{154}Gd for which uncertainties reach 9.75% and 19.98%, respectively.

The most important contributors of uncertainties on nuclide density of ^{243}Am, ^{244}Cm, ^{155}Eu and ^{155}Gd are analyzed at 10, 30 and 50 GWd/tU for the LWR pin-cell. It can be seen from the Fig. 7(a) and (b) that the uncertainties of ^{243}Am and ^{244}Cm are mainly induced by capture cross section of ^{242}Pu. The primary reason is that the covariance data of the capture cross section of ^{242}Pu is considerable, which is shown in Fig. 6(c). As shown in Fig. 7 (c) and (d), the uncertainties on nuclide density of ^{155}Eu and ^{155}Gd are mainly caused by large uncertainty of the capture cross section of ^{155}Eu. The most important contributors of uncertainties on nuclide density of ^{236}U, ^{238}Pu, ^{134}Cs and ^{154}Gd are analyzed for the FR pin-cell. The numerical results are presented in Fig. 8. For ^{236}U, the uncertainty is mainly caused by the capture cross section of ^{235}U, and the uncertainty on ^{238}Pu mainly comes from the capture cross section of ^{237}Np. The uncertainties induced by the capture cross section of ^{133}Cs and ^{153}Eu are the most important source of ^{134}Cs and ^{154}Gd uncertainties, respectively.

In addition, the uncertainties on nuclide density are very different for some isotopes in the different pin-cells, such as ^{238}Pu and ^{154}Gd. The primary reason is that the sensitivity coefficients are different. As shown in Fig. 9, the nuclide density of ^{238}Pu is more sensitive to the ^{237}Np (n, γ) at the lower energy range in the LWR pin-cell. However, it is more sensitive at the higher energy range in FR pin-cell. The covariance data of ^{237}Np (n, γ) shown in Fig. 6(d) is obviously larger at the higher energy range than that at the lower energy range, so the uncertainty of nuclide density of ^{238}Pu induced by the ^{237}Np (n, γ) is larger in the FR pin-cell than that in the LWR pin-cell. Similarly, according to the sensitivity coefficient shown in Fig. 10 and covariance data shown in Fig. 6(b), it is easy to understand that the uncertainty of nuclide density of ^{154}Gd is larger in the FR pin-cell than that in the LWR pin-cell.

4. Conclusions

In this paper, a code named SUNDEW has been successfully developed to assess the sensitivity coefficients and uncertainties induced by the nuclear cross sections uncertainties in the depletion calculation. The verification results show the calculation sensitivity coefficients of SUNDEW agree well with the results of direct perturbation calculation. The sensitivity analysis was performed on K_{eff} and nuclide density with respect to the nuclear cross sections for the LWR and FR pin-cell. At beginning of lifetime, K_{eff} is more sensitive to the cross sections of ^{235}U and ^{238}U. With the depletion of uranium and accumulation of plutonium, the sensitivity coefficient of K_{eff} to the cross sections of ^{235}Uand ^{238}U decreases gradually, while it is growing slowly for the Pu cross sections.

The uncertainties on K_{eff} and nuclide density are quantified based on the covariance data of ENDF/B-VII.1 for the LWR and FR pin-cell. The total uncertainty on K_{eff} at beginning of lifetime amounts to 508pcm and approximately 430 pcm at 60 GWd/tU for the LWR pin-cell. The K_{eff} uncertainty is mainly caused by the nuclear data of ^{235}U and ^{238}U at beginning of lifetime, especially the capture cross section of ^{238}U. With the depletion of uranium and accumulation of plutonium, the plutonium nuclear data become the dominant contributor to the K_{eff} uncertainty. For the FR pin-cell, the total uncertainty on K_{eff} is approximately 2300 pcm at the beginning of the lifetime, which increases gradually with the depth of depletion. The K_{eff} uncertainty mainly comes from the capture of ^{235}U during the whole lifetime. The primary reason is that the K_{eff} is more sensitive to the ^{235}U (n, γ) at the higher energy range than that at the lower energy range in the FR pin-cell, and the covariance data of ^{235}U (n, γ) is obviously larger at the higher energy range than that at the lower energy range.

The uncertainties of nuclide density in the LWR pin-cell are less than 5% for heavy isotopes and 7% for fission products, some exceptions are ^{243}Am, ^{244}Cm, ^{155}Eu and ^{155}Gd for their uncertainties amount to 11.45%, 12.09%, 28.06% and 25.84%, respectively. In the FR pin-cell, the uncertainties of the most heavy isotopes are larger than those in the LWR pin-cell. The uncertainty of ^{236}U is up to 16.11%. In addition, the uncertainties of nuclide density are very different for some isotopes in different pin-cells, such as ^{236}U, ^{238}Pu and ^{154}Gd.

This paper assesses the uncertainties of K_{eff} and the nuclide density induced by the uncertainties of the nuclear cross sections in the depletion calculation. Future investigation on the uncertainties of other response functions will be performed based on the SUNDEW in the future.

Acknowledgement

This work was supported by the National Natural Science Foundation of China No. 11522544.

References

Aliberti, G., Palmiotti, G., Salvatores, M., 2002. The ERANOS code and data system for fast reactor neutronic analyses, Proc. PHYSOR 2002 Conference, October, Seoul, Korea.

Chadwick, M.B., Herman, M., Oblozinsky, P., et al., 2011. ENDF/B-VII.1 nuclear data for science and technology: cross sections, covariance, fission product yields and decay data. Nucl. Data Sheets 112, 2887–2996.

Diez, C.J., Buss, O., Hoefer, A., et al., 2015. Comparison of nuclear data uncertainty propagation methodologies for PWR burn-up simulations. Ann. Nucl. Energy 77, 101–114.

Du, X., Wu, H., Zheng, Y., 2014. The application of Monte Carlo method in fast reactor assembly homogeneous constant calculation. Nucl. Power Eng., S2-0067-04, in Chinese

Ivanov, K., Avramova, M., Kamerow, S., et al., 2012. Benchmark for Uncertainty Analysis in Modeling (UAM) for Design, Operation and Safety Analysis of LWRs. NEA/NSC/DOC.

Koning, A.J., Rochman, D., 2009. TENDL-2009: Consistent Talys-based Evaluated Nuclear Data Library Including Covariances, OECD/NEA JEF/DOC-1310.

Li, Y., Tian, C., Zheng, Y., et al., 2015. NECP-CACTI: Pressurized Water Reactor Lattice Code Development, Transactions of the American Nuclear Society, vol. 112, San Antonio.

MacFarlane, R., Muir, D., 1994. The NOJY Nuclear Data Procession System Version 91. Los Alamos National Laboratory.

Oak Ridge National Laboratory, 2009. SCALE: A Modular Code System for Performing Standardized Computer Analysis for Licensing Evaluation, ORNL/TM-2005/39, Version 6.0. Oak Ridge, Tennessee, USA.

Palmiotti, G., Salvatores, M., Assawatoongruengchot, M., 2009. Nuclear Data for Innovative Fast Reactors: Impact of Uncertainties and New Requirements, International Conference on Fast Reactors and Related Fuel Cycles (FR09)-Challenges and Opportunities.

Pusa, M., 2012a. Incorporating sensitivity and uncertainty analysis to lattice physics code with application to CASMO-4. Ann. Nucl. Energy 40 (1), 153–162.

Pusa, M., 2012. Correction to Partial Fraction Decomposition Coefficients for Chebyshev Rational Approximation on the Negative Real Axis. <http://arxiv.org/abs/1206.2880>.

Pusa, M., Leppanen, J., 2010. Computing the matrix exponential in burnup calculations. Nucl. Sci. Eng. 164, 140–150.

Rearden, B.T., 2004. Perturbation theory eigenvalue sensitivity analysis with Monte Carlo techniques. Nucl. Sci. Eng. 146, 367–382.

Rochman, D., Sciolla, C.M., 2012. Total Monte Carlo Uncertainty Propagation Applied to the Phase I-1 Burnup Calculation, Technical Report, NRG Report 113696.

Salvatores, M., Jacqmin, R., 2008. OECD/NEA WPEC Subgroup 26 Final Report: Uncertainty and Target Accuracy Assessment for Innovative Systems Using Recent Covariance Data Evaluations.

Shibata, K., Iwamoto, O., Nakagawa, T., et al., 2011. JENDL-4.0: a new library for nuclear science and engineering. J. Nucl. Sci. Technol. 48 (1), 1–30.

Takeda, T., Umano, T., 1985. Burn-up sensitivity analysis in a fast breeder reactor - Part I: Sensitivity calculation method with generalized perturbation theory. Nucl. Sci. Eng. 91, l–10.

Williams, M.L., 1978. Development of Depletion Perturbation Theory for Coupled Neutron/Nuclide Fields, Engineering Physics.

Yokoyama, K., 2014. Development and Verification of Three-Dimensional Hex-Z Burnup Sensitivity Solver Based on Generalized Perturbation Theory. Physor 2014, Kyoto, Japan.

Zwermann, W., Krzykacz-Hausmann, B., Gallner, et al., 2012. Aleatoric and epistemic uncertainties in sampling based nuclear data uncertainty and sensitivity analyses, In: Int. Conf. PHYSOR 2012: Conference on Advances in Reactor Physics, 15–20 Apr 2012.